A dielectric-modulated field-effect transistor for biosensing

HYUNGSOON IM, XING-JIU HUANG, BONSANG GU AND YANG-KYU CHOI*

Nano-Oriented Bio-Electronic Lab, School of Electrical Engineering and Computer Science, Korea Advanced Institute of Science and Technology, Daejeon 305-701, Republic of Korea
*e-mail: ykchoi@ee.kaist.ac.kr

Published online: 24 June 2007; doi:10.1038/nnano.2007.180

Interest in biosensors based on field-effect transistors (FETs), where an electrically operated gate controls the flow of charge through a semiconducting channel, is driven by the prospect of integrating biodetection capabilities into existing semiconductor technology[1]. In a number of proposed FET biosensors, surface interactions with biomolecules in solution affect the operation of the gate or the channel[2–19]. However, these devices often have limited sensitivity. We show here that a FET biosensor with a vertical gap is sensitive to the specific binding of streptavidin to biotin. The binding of the streptavidin changes the dielectric constant (and capacitance) of the gate, resulting in a large shift in the threshold voltage for operating the FET. The vertical gap is fabricated using simple thin-film deposition and wet-etching techniques. This may be an advantage over planar nanogap FETs, which require lithographic processing[20–24]. We believe that the dielectric-modulated FET (DMFET) provides a useful approach towards biomolecular detection that could be extended to a number of other systems.

The DMFET nanogap device (Fig. 1a) was fabricated using conventional complementary metal oxide semiconductor (CMOS) processes. The silicon body of the DMFET, consisting of the channel and source and drain electrodes, was formed on a p-doped silicon-on-insulator (SOI) wafer. A 10-nm layer of silicon oxide was grown on the active silicon area to form the gate oxide, followed by 15 nm of chromium and 100 nm of gold to form the gate electrode. The chromium was wet-etched to carve out a 15-nm vertical nanogap underneath the gold layer (see cross-section in Fig. 1b). The length of the nanogap, which defines how deep the channel is etched on either side, varied between 100 and 400 nm. Electron microscopy images of nanogaps with gap lengths of 200 and 400 nm are shown in Fig. 1c,d, respectively. (For further details about the fabrication process, see Methods, and for a schematic diagram of the processing steps, see the Supplementary Information, Fig. S1.)

In this study, we focused on using the DMFET to detect the biotin–streptavidin system because it has one of the highest free energies of association for a non-covalent bond between a protein (streptavidin) and a small ligand (biotin) in aqueous solution. This biomolecular system is also useful in the diagnosis of certain diseases. Assembling the biomolecules in the nanogap requires three steps. First, the cleaned DMFET device is placed into 11-amino-1-undecanethiol hydrochloride solution to form a self-assembled monolayer (SAM) between the amino groups and the exposed gold surface that ultimately serves to anchor the biotin molecules to the walls of the nanogap. Second, the device is immersed in a sulpho-NHS-LC-biotin carbonate buffer solution for 4 h at 4 °C to fix the biotin molecules to the nanogap surface with high stability. Finally, the freshly biotinylated device is immersed in a 300-nM streptavidin/PBST solution for 4 h at 4 °C. The streptavidin is immobilized in the nanogap by strong intermolecular attractions with the biotin.

The surface properties of the assembly were characterized using an atomic force microscope (AFM; see Supplementary Information, Fig. S2a,b). Because of the difficulty in obtaining AFM images of the gold surface inside the nanogap, we performed AFM measurements on exposed gold surfaces prepared in an identical manner to the procedure described above. After assembling the biotin–streptavidin, the surface has a greater mean roughness, $R_a = 0.622$ nm, compared with bare gold, $R_a = 0.162$ nm. Additional information can be obtained from cross-sections of the samples (see Supplementary Information, Fig. S2c). Attenuated total reflectance Fourier transform infrared (ATR-FTIR) spectroscopy (see Supplementary Information, Fig. S2d) further confirms the biotin–streptavidin binding. Peaks in the FTIR spectra corresponding to the C–H, C=O, C–N, C–S, C–C–C and ring stretching vibrations as well as the N–H bend vibration originate from the biomolecules.

In a typical FET device, electric current flows between the source and drain electrodes when the voltage applied to the gate exceeds a threshold voltage (V_T). V_T depends on the gate capacitance, and hence we can modulate V_T by changing the dielectric material of the gate. When the chromium layer is etched to form an air gap, the dielectric constant of the gate and the total gate capacitance are decreased. As a result, V_T for the transistor shifts to a more positive value. In contrast, when biomolecules are introduced into the nanogap, they increase the gate capacitance relative to the air gap, and V_T shifts in the negative direction. Thus, by monitoring the change in V_T, it is possible to detect the specific binding of streptavidin to biotin.

To test this concept, the electrical characteristics of the DMFET in which the nanogap is filled with a weak dielectric (low-k) material were simulated using the ATLAS software[25] (Fig. 2a). In the simulation, which shows how the drain–source current (I_{DS}) varies with the gate voltage (V_{GS}), we filled the device nanogap with a

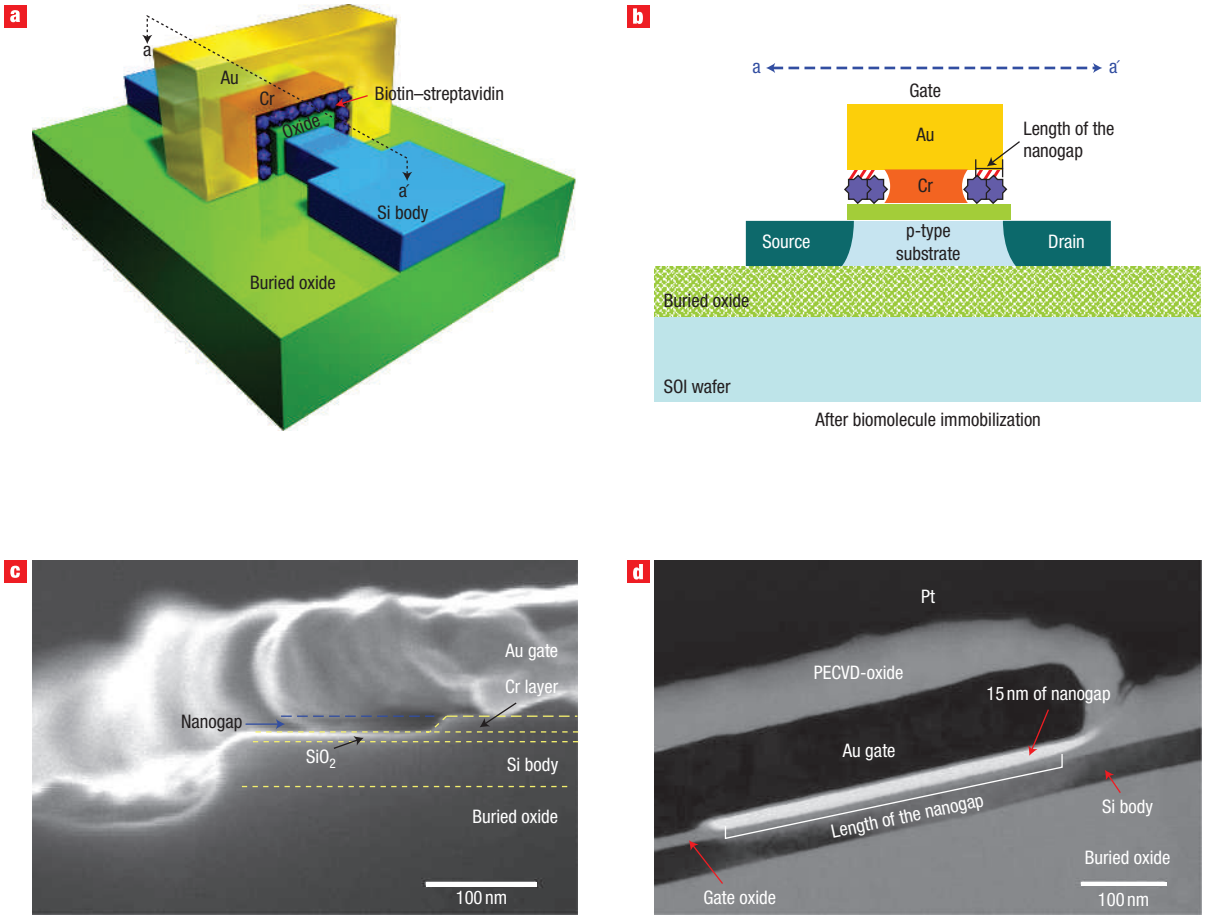

Figure 1 A DMFET. a, Three-dimensional structure showing the silicon body (blue), the gate oxide (green) and the chromium (orange) and gold (yellow) electrodes. The narrow region of the silicon body forms the active silicon region (the channel). The chromium layer is partially etched to form an air gap that can be filled with biomolecules. **b**, A cross-section of the device along the direction of the dotted line in **a** shows the filled nanogap. Source and drain electrodes are formed by implanting phosphorous in the silicon body. **c**, Scanning electron micrograph of a 200-nm-long nanogap. **d**, Transmission electron micrograph (TEM) of a 400-nm-long nanogap. To reduce damage from the electron beam, a SiO_2 layer (PECVD-oxide) is deposited on the gold layer using plasma-enhanced chemical vapour deposition (PECVD). Platinum is deposited as a background material of TEM. In the image, platinum and gold appear black due to their high atomic number, and the nanogap region appears white.

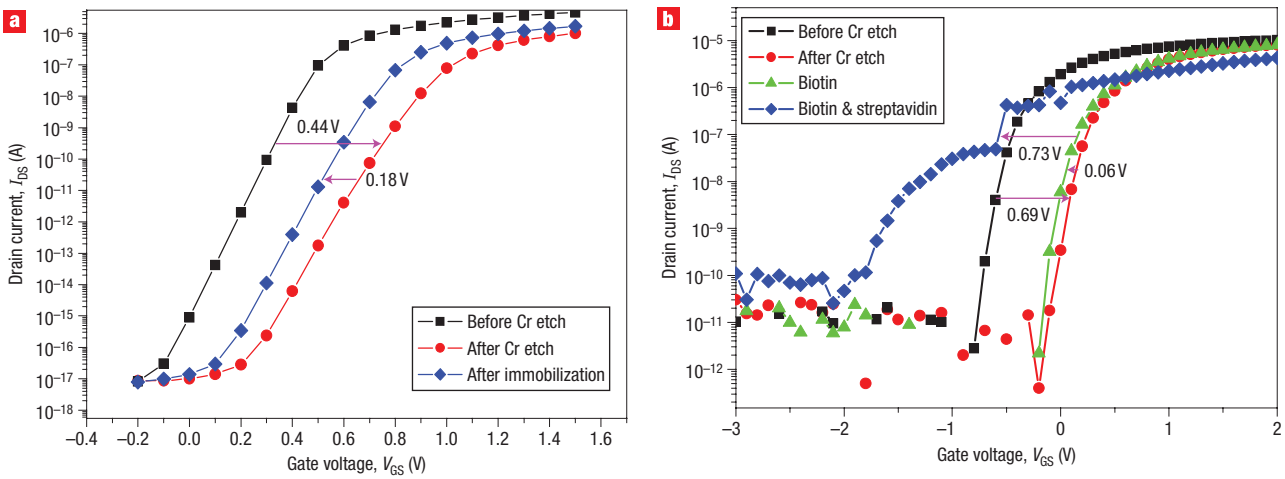

Figure 2 I_{DS}–V_{GS} characteristics of the DMFET nanogap device. a, Results of simulation with low-k materials. **b**, Experimental results at $V_{DS} = 0.05$ V.

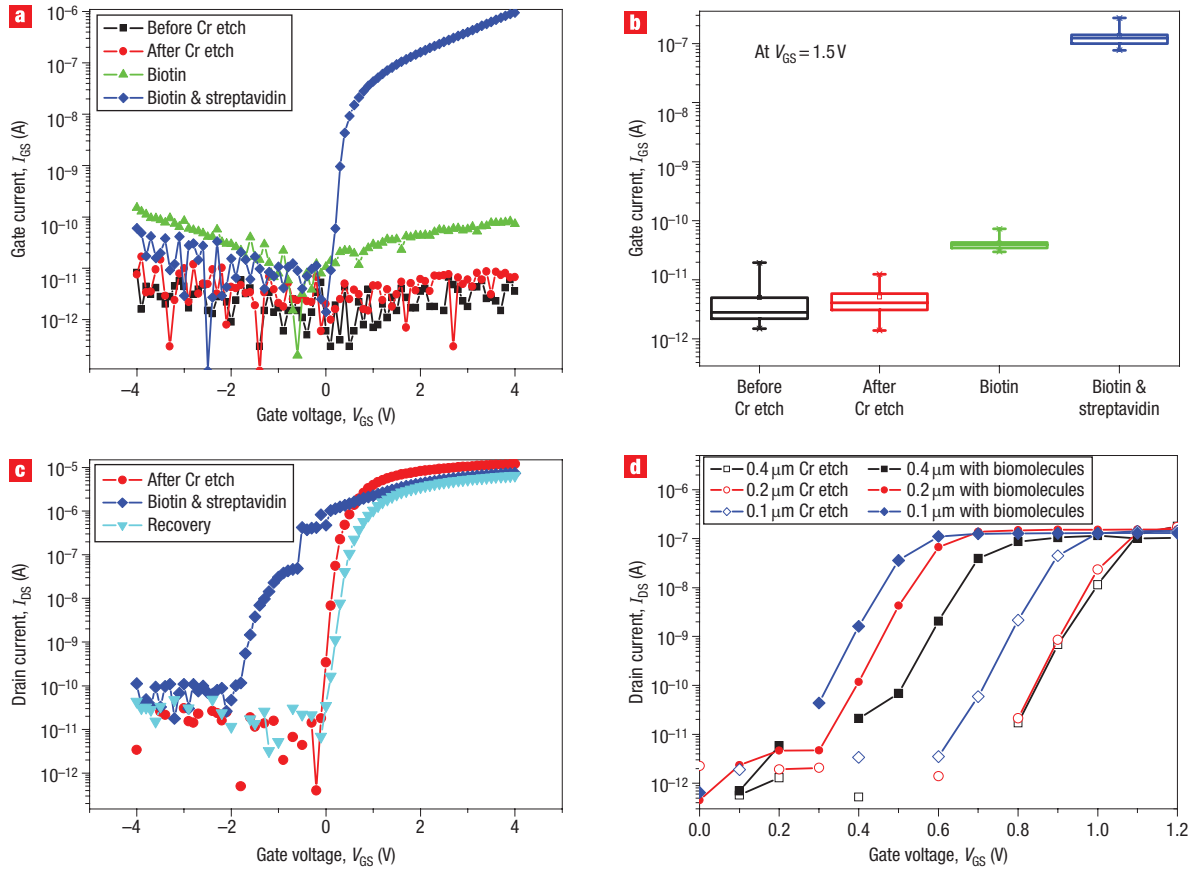

Figure 3 Electrical characteristics of the DMFET nanogap device before and after biomolecules are immobilized in the nanogap. a, I_{GS}–V_{GS} characteristics in one device at V_{DS} = 0.05 V. **b**, Statistical distribution of I_{GS} measured in 15 different devices with V_{GS} = 1.5 V. **c**, I_{DS}–V_{GS} characteristic changes after breaking the biotin–streptavidin binding at V_{DS} = 0.05 V. **d**, The threshold voltage depends on the laterally etched length of the DMFET nanogap devices.

material with $k = 2.1$ to model the presence of the biomolecules[26]. The simulations predict a +0.44 V shift in V_T when the chromium layer is etched to form a 400-nm-long air gap under the Au gate, followed by a shift of −0.18 V when the gap is filled with the low-k dielectric material. Figure 2b shows the I_{DS}–V_{GS} characteristics at different stages of forming and filling the nanogap with biomolecules of an actual DMFET nanogap device with gap length of 200 nm. All measurements are performed at 0.05 V of source–drain voltage (V_{DS}). After etching the 200-nm-long nanogap into the Cr layer, V_T shifts by +0.69 V, because the total gate capacitance decreases by forming additional new air gaps on the gate dielectric at the edge of the gate, which can lead to fringing capacitance. After forming the SAM and immobilizing the biotin, V_T shifts by only −0.06 V as a result of the increase in gate capacitance at the gold side of the inner walls of the air gap. Because the thicknesses of the SAM and biotin layer are about 1–2 nm and 3 nm, respectively, less than 30% of the air gap is filled in the vertical direction, and the increase in gate capacitance and corresponding shift in V_T are relatively small. In contrast, V_T shifts dramatically by −0.73 V after the streptavidin binds to the biotin layer in the nanogap. Considering that streptavidin molecules are about 6–7 nm in size, most of the 15-nm nanogap is filled when the streptavidin binds to the biotin, and the shift in V_T is much larger than in the case of biotin immobilization in the previous step. The decrease in I_{DS} at 1.5 V of V_{GS} is likely due to a higher gate leakage current.

The electrical characteristics of the DMFET nanogap device before and after the biomolecules are immobilized in the nanogap are reported in Fig. 3. Figure 3a shows how the gate leakage current (I_{GS}) depends on the gate voltage in the same device as in Fig. 2b. Before immobilizing the streptavidin, the gate leakage current is in the range of picoamperes, but it increases dramatically to microamperes after biotin–streptavidin binding. We believe that this is because the bound molecules provide a current path for electrons to flow to the gate. A statistical analysis on 15 devices of how the gate current varies with the material in the nanogap is shown in Fig. 3b and is in agreement with previously reported results on biotin–streptavidin binding[27].

Further confirmation that the large threshold voltage change is caused by the specific biotin–streptavidin binding is found by looking at the effects of breaking the binding. The biotin–streptavidin binding can be reversibly and efficiently broken with non-ionic aqueous solutions and brief exposure to high temperature (70 °C) (ref. 28). We immersed the device in hot deionized water (70 °C) for 8 min, and washed it with deionized water several times. As shown in Fig. 3c, the threshold voltage is reversibly shifted to its original state value after breaking the biotin–streptavidin binding. From this experiment, we concluded that the negative threshold voltage shift in the previous experiments can be attributed to the specific biotin–streptavidin binding.

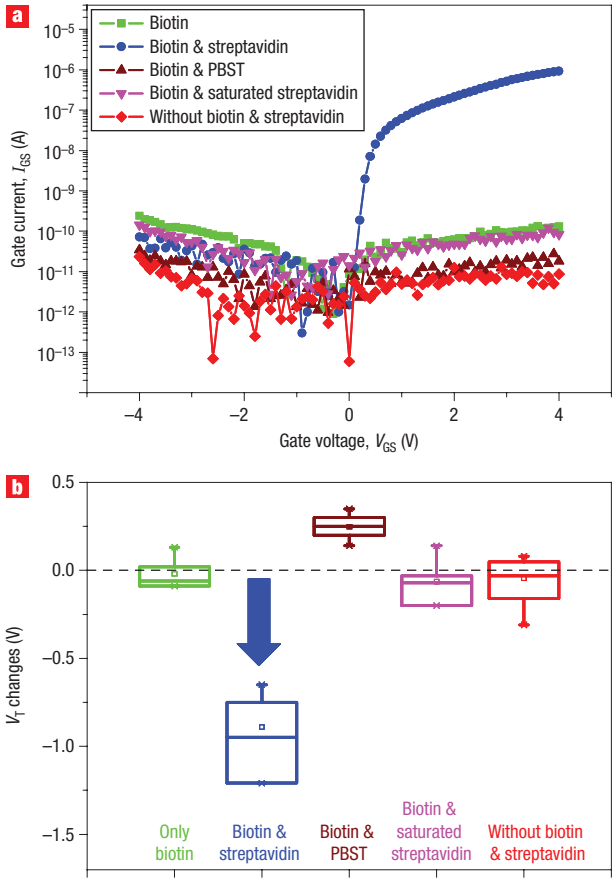

Figure 4 Comparison of the electrical characteristics of the DMFET nanogap device (gap size, 15 nm; length, 200 nm) in five controlled experiments. a, Statistical results of threshold voltage change in all devices. The data set for each group was extracted from 15 devices. **b**, I_{GS}–V_{GS} characteristics at $V_{DS} = 0.05$ V in one device.

Devices with nanogap lengths equal to 100, 200 and 400 nm were studied to confirm that the solution containing biomolecules flows into and fills the nanogap. After biotin–streptavidin binding, the changes of the threshold voltage showed almost the same tendency for all devices (Fig. 3d). In addition, experiments (Fig. 3d) and simulations (see Supplementary Information, Fig. S3) indicate that a nanogap of 200 nm length on either side is sufficient to detect biomolecules by means of the threshold voltage change. However, it is also important to point out that the nanoscale size of the gap has a significant effect on the electrical characteristics of the FET. Fluid flow in narrow (nanoscale) channels is expected to exhibit fundamentally different behaviour from that in macroscopic devices, and further research on size-dependent effects in our devices would be of value and is in hand.

To check that the dramatic current and threshold voltage changes in the biotin–streptavidin binding group do not result from the effects of the buffer solution (such as a shift in V_T resulting from mobile K^+ or Na^+ ions), we analysed the statistical results of threshold voltage changes in 15 nanogap devices (Fig. 4a) and the I_{GS}–V_{GS} characteristics at $V_{DS} = 0.05$ V in one nanogap device (Fig. 4b) with five different groups: biotin, biotin–streptavidin, biotin and PBST, which contain the effects of the buffer solution, biotin-saturated streptavidin, and streptavidin without biotin. We found that only the biotin–streptavidin group shows the large V_T change. From the changes in V_T values, therefore, we suggest that biotin–streptavidin binding is the critical factor for changing the electrical characteristics of the DMFET device. Thus, it is concluded that the DMFET device shows high specificity for detecting biotin–streptavidin binding.

In summary, we have demonstrated a dielectric-modulated field-effect transistor coupled with a 15-nm vertical nanogap that detects the binding of streptavidin to biotin using an all-electrical, CMOS-compatible technique, without the need for a labelling process. The proposed device shows much better sensitivity than several previously reported FET nanogap biosensors[29] for detecting biomolecules, especially protein–ligand binding. Furthermore, by measuring data after breaking the biotin–streptavidin binding and from control group experiments, we verified that biotin–streptavidin binding is the dominant factor in determining the shift in the threshold voltage. In addition, it is expected that such DMFET-type biosensors will have the capability to detect a number of protein molecules, such as DNA, cancer markers and antibodies, and could be used as a part of a lab-on-a-chip for full electronic detection.

METHODS

FABRICATION PROCESS

The starting material was a p-doped SOI wafer, with a 3,000-Å layer of buried oxide and a 1,000-Å layer silicon body on the buried oxide. The thickness of the silicon body was reduced to 500 Å by iterative thermal oxidation and a wet-etching process by buffered oxide etchant (BOE), four times, in order to obtain a conformal silicon body thickness. After silicon body thinning, optical lithography with a wavelength of 436 nm and AZ4330 positive photoresist was used to pattern the active region. The active region was then defined by wet-etching of the silicon body with diluted 10:1 TMAH for 45 s at 57 °C (ref. 30). The gate region was patterned on the active region by optical lithography with AZ4330 photoresist, and the photoresist patterns were used as a hard mask for the subsequent implantation process. Source and drain were defined by phosphorous implantation. The optimal implant energy was determined to be 20 keV to obtain a fully depleted source and drain, and the dose was set to 2×10^{15} cm^{-2}. Impurities were activated by rapid temperature activation (RTA) for 30 s at 1,000 °C.

In order to define the gate region, a 10-nm gate oxide was grown by thermal dry oxidation for 4 min at 1,000 °C, and 15-nm Cr and 100-nm Au layers were respectively deposited by evaporation on the silicon body, in order. Other kinds of oxides, such as HfO_2 and Al_2O_3 deposited by atomic layer deposition, can also be used as a gate oxide. The base pressure of the vacuum chamber was lower than 1×10^{-6} torr. To deposit Cr and Au layers, electron-beam evaporation and thermal evaporation were used, respectively. The deposition rate of Cr was ~0.3 Å s^{-1} and that of Au ~0.5 Å s^{-1}. In the next process, an extremely thin layer of Cr deposited by electron-beam evaporation was used to determine the size of the vertical nanogap. The size of this vertical nanogap should be changed to correspond to the size of biomolecules to be detected. After deposition of the gate layers, optical lithography with AZ6612K positive photoresist was used to define the gate electrode. After the positive photoresist patterns were formed, Au, Cr and oxide layers were etched by a wet-etching process. To etch Au, Cr and the oxide layer, 10:1 diluted KCN solution, Cr etchant and BOE were used, respectively. The device fabricated by the above process was alloyed in an alloy furnace for an hour at 400 °C under a flow of 95% H_2 forming gas.

Finally, the Cr layer was laterally etched by Cr etchant without agitation. The gap size was determined by the thickness of the Cr layer, and the nanogap length was ~200 nm after etching with Cr etchant for 6 min.

PROCEDURES FOR BIOTIN–STREPTAVIDIN BINDING

Streptavidin and 11-amino-1-undecanethiol hydrochloride were purchased from Sigma-Aldrich. The 11-amino-1-undecanethiol hydrochloride solution was prepared by dissolving in ethanol and the concentration was adjusted to 3 mM. Sulpho-NHS-LC-biotin (Pierce) solution was prepared in a 0.1 M sodium carbonate solution and the concentration was adjusted to 3 mM. Double

deionized water (DDW) was used in all measurements. A phosphate-buffered saline solution (PBS, pH 7.4) was prepared by dissolving 1.6 g of KCl, 64 g of NaCl, 1.92 g of KH_2PO_4 and 11.52 g of K_2HPO_4 in 800 ml of DDW (all from Junsei Chemical Co.). PBST solution was prepared using PBS solution and 0.05% Tween20 (Sigma-Aldrich).

Prior to assembly, the nanogap device was cleaned thoroughly with acetone and DDW and dried in a stream of high-purity N_2. The cleaned nanogap device was then placed into 11-amino-1-undecanethiol hydrochloride solution at room temperature, followed by exhaustive washing using ethanol and DDW 4 h later, after which it was blow dried.

The nanogap device with SAM was then placed into a sulpho-NHS-LC-biotin carbonate buffer solution for 4 h at 4 °C followed by DDW and PBST washing. It is necessary to point out here that the biotinylation solution must be prepared freshly each time it is required due to the quick hydrolysis of the NHS esters. After being rinsed with DDW and PBST, the fresh biotinylation device was immersed into a 300 nM streptavidin/PBST solution for another 4 h at 4 °C, followed by washing using PBST and DDW and blow drying in ultra-pure nitrogen.

To break the biotin–streptavidin binding, we immersed the device in hot DDW (70 °C) for 8 min, and washed it with DDW several times.

EXPERIMENTAL MEASUREMENT METHOD

The bindings of the SAM, biotin and streptavidin were detected by measuring the change in the electrical characteristics of the DMFET device, including the threshold voltage (V_T) shift, using the semiconductor parameter analyser (HP4156C).

The electrical characteristics of the DMFET device were measured after each immobilization step, in other words by measuring the data after immobilization of the SAM, biotin and streptavidin, respectively.

The gate, drain and source currents were measured while the gate voltage was swept from −4 V to 4 V with the source grounded and a voltage of 50 mV applied to the drain. All measurements were performed on the probe station. The voltages were applied through probing tips that were directly in contact with each probing pad in the device and fixed by vacuum. The currents were measured through the probing tips while the corresponding voltage was applied.

FESEM and TEM images were obtained with a Philips XL 30 AFEG scanning electron microscope and FEI Tecnai F20, respectively. Atomic force microscopy images were carried out using Nanoscope III (Digital Instruments, Veeco Metrology). ATR-FTIR spectroscopy was performed using an IFS 66v/S Vacuum FT-IR, ATR mode (Bruker Optics).

Received 22 January 2007; accepted 21 May 2007; published 24 June 2007.

References

1. Kim, D. S. *et al.* An extended gate FET-based biosensor integrated with a Si microfluidic channel for detection of protein complexes. *Sens. Actuator B* **117,** 488–494 (2006).
2. Purushothaman, S., Toumazou, C. & Ou, C. P. Protons and single nucleotide polymorphism detection: A simple use for the ion sensitive field effect transistor. *Sens. Actuator B* **114,** 964–968 (2006).
3. Shekhawat, G., Tark, S. H. & Dravid, V. P. MOSFET-embedded microcantilevers for measuring deflection in biomolecular sensors. *Science* **311,** 1592–1595 (2006).
4. Wang, W. U., Chen, C., Lin, K. H., Fang, Y. & Lieber, C. M. Label-free detection of small-molecule–protein interactions by using nanowire nanosensors. *Proc. Natl Acad. Sci. USA* **102,** 3208–3212 (2005).
5. Xiang, J. *et al.* Ge/Si nanowire heterostructures as high-performance field-effect transistors. *Nature* **441,** 489–493 (2006).
6. Cui, Y., Wei, Q. Q., Park, H. K. & Lieber, C. M. Nanowire nanosensors for highly sensitive and selective detection of biological and chemical species. *Science* **293,** 1289–1292 (2001).
7. Patolsky, F. *et al.* Electrical detection of single viruses. *Proc. Natl Acad. Sci. USA* **101,** 14017–14022 (2004).
8. Li, C. *et al.* Chemical gating of In_2O_3 nanowires by organic and biomolecules. *Appl. Phys. Lett.* **83,** 4014–4016 (2003).
9. Bradley, K., Cumings, J., Star, A., Gabriel, J. C. P. & Grüner, G. Influence of mobile ions on nanotube based FET devices. *Nano Lett.* **3,** 639–641 (2003).
10. Star, A. *et al.* Label-free detection of DNA hybridization using carbon nanotube network field-effect transistors. *Proc. Natl Acad. Sci. USA* **103,** 921–926 (2006).
11. Star, A., Gabriel, J. C. P., Bradley, K. & Grüner, G. Electronic detection of specific protein binding using nanotube FET devices. *Nano Lett.* **3,** 459–463 (2003).
12. Star, A., Han, T. R., Gabriel, J. C. P., Bradley, K. & Grüner, G. Interaction of aromatic compounds with carbon nanotubes: correlation to the Hammett parameter of the substituent and measured carbon nanotube FET response. *Nano Lett.* **3,** 1421–1423 (2003).
13. Star, A., Han, T. R., Joshi, V., Gabriel, J. C. P. & Grüner, G. Nanoelectronic carbon dioxide sensors. *Adv. Mater.* **16,** 2049–2052 (2004).
14. Javey, A., Guo, J., Wang, Q., Lundstrom, M. & Dai, H. J. Ballistic carbon nanotube field-effect transistors. *Nature* **424,** 654–657 (2003).
15. Keren, K., Berman, R. S., Buchstab, E., Sivan, U. & Braun, E. DNA-templated carbon nanotube field-effect transistor. *Science* **302,** 1380–1383 (2003).
16. Stutzmann, N., Friend, R. H. & Sirringhaus, H. Self-aligned, vertical-channel, polymer field-effect transistors. *Science* **299,** 1881–1884 (2003).
17. Naber, R. C. G. *et al.* High-performance solution-processed polymer ferroelectric field-effect transistors. *Nature Mater.* **4,** 243–248 (2005).
18. Muccini, M. A bright future for organic field-effect transistors. *Nature Mater.* **5,** 605–613 (2006).
19. Oprea, A. *et al.* Copper phthalocyanine suspended gate field effect transistors for NO_2 detection. *Sens. Actuator B* **118,** 249–254 (2006).
20. Krahne, R. *et al.* Nanoparticles and nanogaps: controlled positioning and fabrication. *Physica E* **17,** 498–502 (2003).
21. Iqbal, S. M., Balasundaram, G., Ghosh, S., Bergstrom, D. E. & Bashir, R. Direct current electrical characterization of ds-DNA in nanogap junctions. *Appl. Phys. Lett.* **86,** 153901–153903 (2005).
22. Ionescu-Zanetti, C., Nevill, J. T., Carlo, D. D., Jeong, K. H. & Lee, L. P. Nanogap capacitors: Sensitivity to sample permittivity changes. *J. Appl. Phys.* **99,** 024305–024309 (2006).
23. Lazzarino, M. *et al.* Twin cantilevers with a nanogap for single molecule experimentation. *Microelectron. Eng.* **83,** 1309–1311 (2006).
24. Yi, M. Q., Jeong, K. H. & Lee, L. P. Theoretical and experimental study towards a nanogap dielectric biosensor. *Biosens. Bioelectron.* **20,** 1320–1326 (2005).
25. *ATLAS v2002 User's Manual* (Silvaco, Santa Clara, California, 2006).
26. Chen, C. D., Cheng, S. F., Chau, L. K. & Wang, C. R. C. Sensing capability of the localized surface plasmon resonance of gold nanorods. *Biosens. Bioelectron.* **22,** 926–932 (2007).
27. Jang, D. Y. *et al.* Sub-lithographic vertical gold nanogap for label free electrical detection of protein–ligand binding. *J. Vac. Sci. Technol. B* **25,** 443–447 (2007).
28. Holmberg, A. *et al.* The biotin–streptavidin interaction can be reversibly broken using water at elevated temperatures. *Electrophoresis* **26,** 501–510 (2005).
29. Poghossian, A., Cherstvy, A., Ingebrandt, S., Offenhäusser, A. & Schöning, M. J. Possibilities and limitations of label-free detection of DNA hybridization with field-effect-based devices. *Sens. Actuator B* **111–112,** 470–480 (2005).
30. Tabata, O., Asahi, R., Funabashi, H., Shimaoka, K. & Sugiyama, S. Anisotropic etching of silicon in TMAH solutions. *Sens. Actuator A* **34,** 51–57 (1992).

Acknowledgements

This work was supported by the National Research and Development Program (NRDP, 2005-01274) for biomedical function monitoring biosensor development sponsored by the Korea Ministry of Science and Technology (MOST). X.J.H. would like to express appreciation for the financial support of the Brain Korea 21 project, the School of Information Technology, and the Korea Advanced Institute of Science and Technology in 2007. The work was partially supported by the Center for Ultramicrochemical Process Systems, sponsored by KOSEF and Samsung Electronics.

Correspondence and requests for materials should be addressed to Y.K.C.

Supplementary information accompanies this paper on www.nature.com/naturenanotechnology.

Author contributions

Y.K.C. conceived the biosensor application with a dielectric-modulated field-effect transistor. H.I. and Y.K.C. designed the transistor experiments, and H.I. fabricated the transistors. X.J.H. and H.I. performed bio-related experiments, and B.G. worked on simulation. H.I. and X.J.H. co-wrote the paper. All authors contributed data analysis and interpretation equally.

Competing financial interests

The authors declare no competing financial interests.